WORLD OCEAN CIRCULATION

ALGORITHM THEORETICAL BASIS DOCUMENT FOR

NAME OF PRODUCTS (THEME NUMBER)

customer	ESA/ESRIN
ESA contract	ESA Contract No. 4000130730/20/I-NB
document reference	WOC-ESA-ODL-NR-009_T(number)_nameproducts_V1.0
Version/Rev	1.0
Date of issue	28/06/2020.

Distribution List

	Name	Organization	Nb. copies
Sent to:	M.H. Rio	ESA/ESRIN	ESA-STAR
Internal copy:	Fabrice Collard	OceanDatalab	1 (digital copy)

Document evolution sheet

Ed.	Rev.	Date	Purpose evolution	Comments
1	0	28/06/2020	Creation of document	

Contents

List Of Images

List Of Tables

1 Introduction

1.1 Products summary

This Algorithm Theoretical Basis Document (ATBD) describes the first version of the algorithm for retrieving Ocean Surface Current (OSC) Radial Velocity (RVL) from the Sentinel-1 Synthetic Aperture Radar (SAR) Doppler frequency shift observation acquired in the Interferometric Wide (IW) mode VV polarization (Level 2 product).

1.2 Scope & Objectives

This ATBD applies to the ESA World Ocean Circulation (WOC) Project and a part of the deliverable for Theme 1 & 4. The Document provides expert users with the information on the processing required for:

- Calibration of the non-geophysical contributions to the Doppler frequency shift provided in the Sentinel-1 IW Level 2 products;
- Estimation and removal of the sea-state-induced contribution (wave bias) to observed geophysical Doppler frequency shift.

It also describes the Sentinel-1 IW Ocean Surface Current (OSC) Radial Velocity (RVL) product developed for the WOC Project and the preliminary validation of the product using daily gridded geostrophic velocity fields and the Sea Surface Temperature observations, and hourly in situ Lagrangian surface drifter observations in Agulhas Current from May 2019 - April 2020.

1.3 Applicable & Reference documents

[1] Chapron, B., Collard., F., and Ardhuin F.. (2005). Direct measurements of ocean surface velocity from space: Interpretation and validation. *Journal of Geophysical Research,* vol. 110

[2] Johannessen, J. A., Chapron, B., Collard, F., Kudryavtsev, V., Mouche, A., Akimov, D., & Dagestad, F. F. (2008). Direct ocean surface velocity measurements from space: Improved quantitative interpretation of Envisat ASAR observations. *Geophysical Research Letters, 35*, 1-6.

[3] Mouche, A. A. (2012). On the use of doppler shift for sea surface wind retrieval from SAR. *IEEE Transactions on Geoscience and Remote Sensing, 50*(7), 2901-2909.

[4] OceanDataLab. (2019). S-1 RVL DIL4: Algorithm description document. ESRIN: ESA.

[5] Johnsen, H (2016). Ocean doppler anomaly and ocean surface current from Sentinel-1

TOPS mode, in International Geoscience and Remote Sensing Symposium (IGARSS), Beijing, 2016.

[6] Moiseev, A., Johannessen, J.A., Johnsen, H., (2020). Towards Retrieving Reliable Ocean Surface Currents in the Coastal Zone from the Sentinel-1 Doppler Shift Observations. Journal of Geophysical Research: Oceans *(In review)*

[7] Moiseev, A., Johnsen, H., Johannessen, J. A., Collard, F., & Guitton, G. (2020). On removal of sea state contribution to Sentinel-1 Doppler shift for retrieving Reliable Ocean surface current. Journal of Geophysical Research: Oceans, 125, e2020JC016288. https://doi.org/10.1029/2020JC016288

[8] Moiseev, A., Johnsen, H., Hansen, M. W., & Johannessen, J. A. (2020). Evaluation of radial ocean surface currents derived from Sentinel-1 IW Doppler shift using coastal radar and Lagrangian surface drifter observations. Journal of Geophysical Research: Oceans, 125, e2019JC015743. https://doi.org/10.1029/2019JC015743

[8] Elipot, S., R. Lumpkin, R. C. Perez, J. M. Lilly, J. J. Early, and A. M. Sykulski. (2016), A global surface drifter data set at hourly resolution, J. Geophys. Res. Oceans, 121, 2937–2966, doi:10.1002/2016JC011716

1.4 Abbreviations

AEP	Antenna Element Pattern
ATBD	Algorithm Theoretical Basis Document
CMEMS	Copernicus Marine Environment Monitoring Service
ECMWF	European Centre for Medium-Range Weather Forecasts
ESA	European Space Agency
SAR	Synthetic Aperture Radar
SST	Sea Surface Temperature
RVL	Radial velocity
OSC	Ocean Surface current
IW	Interferometric Wide
OCN	Ocean
GMF	Geophysical Model Function
GDP	Global Drifter Program
WW3	Wavewatch III

1.5 Notation

Symbol	Units	Description
f_{dc}	Hz	Observed Doppler Centroid (Doppler frequency shift)
f_{bias}	Hz	Doppler Centroid error due to antenna electronic miss-pointing term
f_{att}	Hz	Doppler Centroid error due to miss-pointing related to satellite attitude
f_{sca}	Hz	Scalloping error due to SAR antenna sweep motion in the TOPSAR mode
f_{osc}	Hz	Doppler shift due to ocean surface current
f_{ss}	Hz	Doppler shift due to sea state bias
f_{rvl}	Hz	Geophysical Doppler shift
β	deg.	Boresight angle
θ_{att}	mdeg.	Attitude deviation from the nominal steering
θ_{y}	mdeg.	Yaw deviation from the nominal attitude
θ_{p}	mdeg.	Pitch deviation from the nominal attitude
θ	deg.	Incidence angle
k_{e}		Radar electromagnetic wavenumber
u_{10}	m/s	Wind speed at 10m height
ϕ	deg.	Wind direction at 10 m height in meteorological convention
x_{10}	m/s	Line-of-sight component of the wind speed at 10m height
f_{c}	Hz	Radar frequency
υ	m/s	Satellite velocity
α_{sar}	deg.	Satellite azimuth (flight) direction

σ_{dc}	Hz	Standard deviation in the observed Doppler frequency shift

2 Ocean surface current radial velocities from the Sentinel-1 Doppler shift

2.1 Background

The satellite Synthetic Aperture Radars (SARs) can provide high-resolution observations of the ocean surface in day-and-night, all-weather conditions. The phase information recorded in the backscatter by SAR can be used to derive the Doppler centroid anomaly (hereafter Doppler shift). This Doppler shift acquired over the ocean contains information about the ocean surface motion induced by the near-surface wind, waves, and ocean surface currents in the radar line-of-sight direction [1, 2, 3, 8].

The Sentinel-1 is an operational constellation of two satellites (A/B) carrying C-Band SAR antennas, operating under the European Space Agency (ESA) Copernicus program, with scheduled performance beyond 2030 (with the launch of two more platforms). Observations acquired by Sentinel-1 in the Interferometric Wide (IW) mode are regularly available in the coastal areas. The Doppler frequency shift observations are routinely provided in the Sentinel-1A/B IW Level 2 OCN Radial Velocity (RVL) products. The signal from the standard products consists of several terms:

$$f_{dc} = f_{bias}(\beta) + f_{att}\left(\beta, \theta_{att}(t)\right) + f_{sca} + \underbrace{\left(f_{osc} + f_{ss}\right)}_{f_{rvl}} + \Delta f \qquad (1)$$

where:

- f_{bias} is the antenna electronic miss-pointing term, related to the gradual degradation of SAR antenna and consequent change of the antenna pattern, yielding deviation from the nominal pointing angle. This term has a distinct pattern within each subswath in the range (across-track) direction and yields "jumps" in the signal between the sub-swaths (e.g., Figure 1a). In the azimuth (along-track) direction the bias is assumed to be stable over several consequent orbits.
- f_{att} is the miss-pointing error due to satellite attitude roll, pitch, and yaw deviations, θ_{att}, from the nominal steering at time t. This signal is rapidly changing in the azimuth direction (e.g., Figure 1b) and is a function of the boresight angle β in the range direction.
- f_{sca} is the scalloping error due to SAR antenna sweep motion in the TOPSAR acquisition mode (e.g., Figure 1c) related to the elevation direction antenna element

pattern (AEP) envelope that weighs the total phased array beam pattern yielding bias in the beam center.

- f_{rvl} is the geophysical signal related to the range component of the ocean surface radial velocity (RVL) that can be approximated as a sum of the sea-state-induced motion (so-called wave bias), f_{ss}, and the underlying ocean surface current, f_{osc}. The $f_{rvl} > 0$ / $f_{rvl} < 0$ indicates the surface motion towards/away from the SAR antenna. The $f_{rvl} = 0\,Hz$ over the land areas.

- Δf is the residual bias related to the inaccurate estimation of the non-geophysical contributions, periodical automatic compensation of the temperature-dependent gain and phase variations of the transmit and receive modules of the Sentinel-1 SAR instrument (e.g., Figure 1c), and other unknown biases.

Therefore, to retrieve the ocean surface current radial velocity from the Sentinel-1 IW Doppler shift observations (i) the f_{dc} must be cleaned from all non-geophysical contributions, (ii) the sea-state-induced part of the observed f_{rvl} must be estimated and removed.

This ATBD describes the first version of the algorithm for deriving Sentinel-1 (S1) Ocean Surface Current (OSC) Radial Velocity (RVL) product including:

- Description of the S1-OSC-RVL product (section 2.2);
- Calibration of the non-geophysical contributions to the signal based on the gyroscope telemetry and observations over land (section 2.3);
- Estimation of the wave bias (section 2.4).

The methodology is applied to the Sentinel-1A/B IW swaths acquired over the South African coastal zone (Agulhas current) in May 2019 - April 2020 with consequent validation of the SAR-derived ocean surface currents based on comparison with daily gridded geostrophic velocities and Sea Surface Temperature fields from the independent satellite remote sensing observations (see section 2.5).

2.2 The Sentinel-1A/B IW OCN RVL product overview

The Sentinel-1A/B Interferometric Wide (IW) Ocean Surface Current (OSC) Radial Velocity (RVL) product is derived from the standard Sentinel-1 IW Level 2 OCN RVL products routinely provided by Copernicus. Each S1-OSC-RVL product covers an area of about 200x250 km with a pixel size of 1x1 km. The product contains Doppler frequency shift observations after removal of the non-geophysical contributions to the signal due to unstable platform attitude, antenna electronic miss-pointing, and scalloping following the methodology described in section 2.3. It also contains the wave bias estimates derived using the CDOPSiX geophysical model function and the wind field at 10 m height from the collocated ECMWF model following the methodology described in section 2.4. In addition to the SAR observations, the product contains wind speed and direction at 10 m height from the ECMWF and Stokes drift from the WW3 with full list of the variables described in Table 1.

Following the data provided in the S1-OSC-RVL products the Doppler shift due to the ocean surface current can be retrieved following:

$$f_{osc} = f_{rvl} - f_{ss} \quad (2)$$

where f_{rvl} is geophysical Doppler frequency shift (see Table 1 *doppler_centroid_anomaly*) and f_{ss} is the sea state bias (see Table 1 *wave_bias*). The Doppler shift can be then converted to the ground range ocean surface current radial velocity following:

$$u_{osc} = \frac{\pi f_{osc}}{k_e \sin\theta} \quad (3)$$

where θ is the incidence angle (see Table 1 *incidence_angle*) and k_e the radar electromagnetic wavenumber.

Table 1 Variables provided in the Sentinel-1 IW OCN RVL product

OSC RVL variable	Description	Units
lon	Longitude at the cell center	degrees east
lat	Latitude at the cell center	degrees north
sigma0	VV polarized radar cross section	dB
doppler_centroid_std	Estimated doppler centroid frequency std	Hz
quality_level	Confidence on Estimated doppler centroid frequency	-
land_area_fraction	Fraction of land coverage within a cell	%
radial_direction	Radial direction of SAR acquisitions (clockwise from north)	degrees
doppler_centroid_anomaly	Geophysical Doppler frequency shift (i.e., after applying all the non-geophysical calibrations)	Hz

incidence_angle	Incidence angle at the cell center	degrees
wave_bias	Estimated Sea State bias	Hz
wind_speed	ECMWF Wind speed	m/s
wind_direction	ECMWF Wind direction (meteorological convention)	degrees
eastward_stokes_drift_velocity	Longitudinal component of surface stokes drift from Wavewatch III model	m/s
northward_stokes_drift_velocity	Meridional component of surface stokes drift from Wavewatch III model	m/s
time	Acquisition time	-

2.3 Calibration of the Sentinel-1 Doppler radial velocity products

The Doppler frequency shift from the standard Sentinel-1 A/B IW L2 OCN RVL products contain a non-geophysical signal that must be removed to access the signal induced by the ocean surface currents. The experimental calibration developed by the OceanDataLab [4] takes advantage of gyroscope telemetry yielding more accurate removal of the attitude error and therefore more accurate geophysical retrievals. The calibration algorithm consists of two steps:

- Removal of the f_{att} using telemetry from gyroscope operating on board of the satellite.
- Removal of the f_{bias} using SAR observations acquired over the land.

The residual signal after the calibration is evaluated using the data acquired over the land areas.

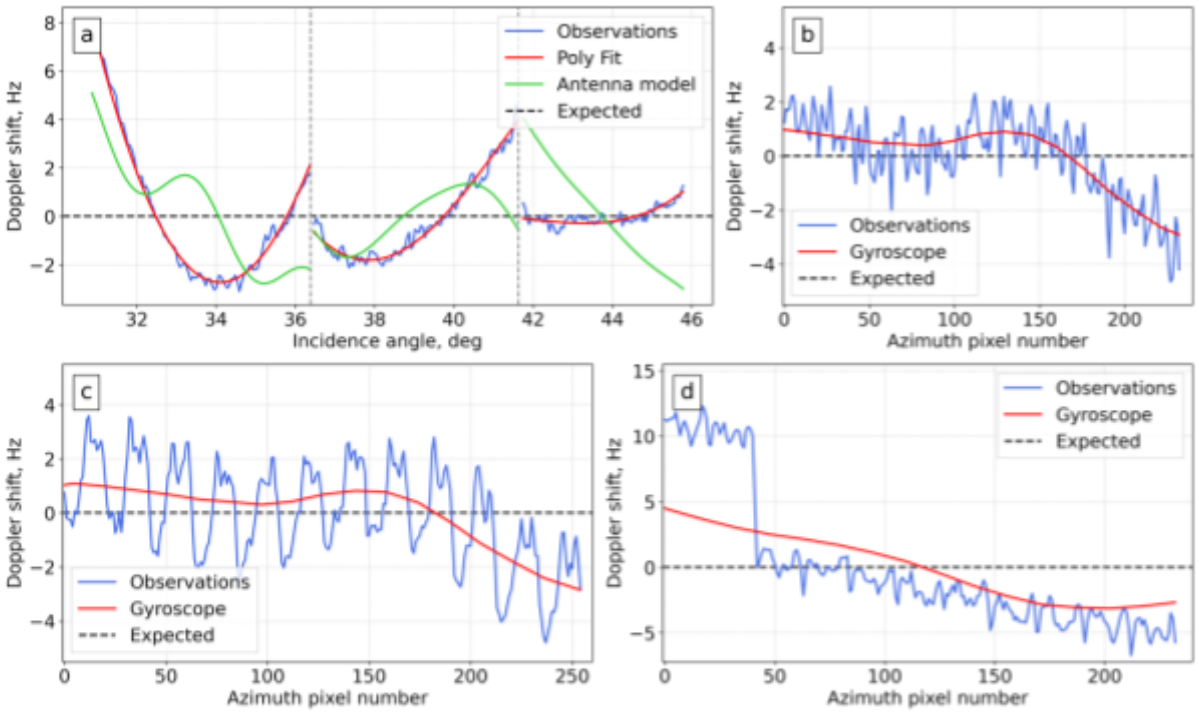

Figure SEQ Figure * ARABIC1. *Doppler shift profiles associated with various non-geophysical contributions to the Sentinel-1 Doppler frequency shift based on observations acquired over the rainforests: (a) Mean range Doppler shift profile from observations (blue) and antenna model (red); Mean azimuth Doppler shift profile from observations (blue) and Doppler error due to attitude variation estimated from the gyroscope telemetry (red) for the 2nd subswath (b) and 1st subswath (c). (d) Mean range Doppler profile from observations (blue) and antenna model (red); Mean azimuth Doppler shift profile from observations (blue) and Doppler error due to attitude variation estimated from the gyroscope telemetry (red) for the 2nd subswath. (a, b, c) are retirieved from Sentinel-1B IW scene on 28 December 2017 at 23:11.19, (d) is from the Sentinel-1B IW scene acquired over the rainforest area on 31 December 2017 at 21:58.50.*

2.3.1 Estimation of the error due to satellite attitude

Following the solution proposed by the [4], the f_{att} in each grid point can be calculated using platform pitch, θ_p, and yaw deviations, θ_y, from the nominal attitude derived from the gyroscope telemetry:

$$f_{att} = \frac{2\upsilon f_c}{c}\left(-\Delta\theta_y \sin sin\,\beta + \Delta\theta_p \cos cos\,\beta\right) \quad (4)$$

where υ is the satellite velocity, f_c is the SAR frequency, and the c is the speed of light. The calculated f_{att} describes the variability in the observed f_{dc} along the azimuth direction as demonstrated in Figure 1b, c.

2.3.2 Estimation of the error due to antenna electronic miss-pointing

Based on the assumption that the $f_{rvl} = 0\,Hz$ over the land, observations acquired over the land areas can be used to estimate the f_{bias} [5]. We used the following algorithm to estimate the f_{bias} in the Sentinel-1 IW swaths on the orbit-by-orbit basis:

1. Estimate the f_{bias} in each pixel over land within the swath as $f_{bias} = f_{dc} - f_{att} - f_{sca}$.
2. Calculate the mean f_{bias} profile in the range direction (e.g., Figure 1a blue).
3. Fit the average f_{bias} profile with a polynomial as a function of the incidence angle (e.g., Figure 1a red).
4. Use the estimated f_{bias} profile for calibration of all observations in the swath, assuming that it does not change within the same orbit.

2.3.3 Calibration and evaluation of the residual signal

Observations acquired over the land areas, especially over the rainforests, are frequently used for the evaluation of the non-geophysical contributions to the f_{dc} because there $f_{rvl} = 0\,Hz$. Analysis of the IW observations acquired over the rainforest areas indicated that the f_{att} is responsible for about 30% of the standard deviation in the Doppler observations, σ_{dc} [6]. We further found that the f_{bias} is responsible for the 15% of the σ_{dc} [6]. Using the acquired f_{bias} and f_{att} estimates the f_{rvl} can be derived as:

$$f_{rvl} = f_{dc} - f_{att} - f_{bias} - f_{sca} \quad (5)$$

After calibration, the residual $\sigma_{dc} \approx 3.8\,Hz$ with the mean bias is close to 0 Hz. The σ_{dc} corresponds to about 0.10 - 0.21 m/s when converted to ground range radial velocity (eq. 3), depending on the incidence angle [6].

2.3.4 Product output

The geophysical Doppler shift (i.e., after the calibration) is delivered in the S1-OCN-RVL product (see Table 2).

Table 2 Output of the calibration step to the S1-OSC-RVL product

S1-OSC-RVL Variable	Description
doppler_centroid_anomaly	Doppler frequency shift after removal of the non-geophysical contributions

2.4 Removal of the wave bias from the geophysical Doppler frequency shift

When all non-geophysical contributions are removed from the f_{dc}, the residual f_{rvl} is the geophysical signal from the ocean surface motion. Previous theoretical studies [2] demonstrated that the f_{rvl} can be approximated as a sum of the signal induced by the sea state, f_{ss}, and the surface current, f_{osc}. Therefore the f_{ss} must be estimated and subtracted from the total geophysical signal in order to derive the ocean surface current radial velocity.

2.4.1 Geophysical Model Function

At the first order the f_{ss} can be approximated as a function of the near-surface wind field, assuming that the sea state at the time of SAR acquisition is in equilibrium with the local wind field [3, 6, 7]. The CDOPSiX is an empirical Geophysical Model Function (GMF) that can predict the f_{ss} based on the wind field from the collocated model and the radar configuration [6]:

$$f_{ss} = CDOPSiX\left(x_{10}, \theta\right) \quad (6)$$

where x_{10} is line-of-sight (hereafter range) directed component of the wind speed at 10 m height, and θ is SAR incidence angle.

2.4.2 Wind transformation

To derive the estimates of the sea state bias in this product we used the wind field from the collocated ECMWF model. To derive the range wind component wind directions were transformed to a coordinate system whereby the directions are defined with respect to the SAR antenna look direction:

$$\phi_{sar} = \phi - \alpha_{sar} - 90° \quad (7)$$

where α_{sar} is the satellite azimuth direction and ϕ is the wind direction from true north. In the SAR coordinate system, 0° denotes the antenna look direction (line-of-sight), while 90° denotes the satellite flight direction (azimuth). Hence, 0° and 180° directions (in the meteorological convention) respectively imply upwind (i.e., the wind blows towards the radar) and downwind (i.e., the wind blows away from the radar), while 90° and 270° represent azimuth winds (i.e., the wind blows along the satellite track). Using the transformed wind direction, we retrieved range directed wind component:

$$x_{10} = u_{10}\, cos(-\phi_{sar} - 90°) \quad (8)$$

where u_{10} is the wind speed.

2.4.3 Product output

The estimates of wave bias from CDOPSiX and wind speed and direction at 10m height from the collocated ECMFW model are provided in the S1-OCN-RVL product (see Table 3).

Table 3 Output of the wave bias estimation step to the S1-OSC-RVL product

S1-OSC-RVL Variable	Description
wave_bias	Estimates of the sea state bias in each grid cell derived using the CDOPSiX GMF model and the ECMWF wind speed
wind_speed	Wind speed at 10m height from the collocated ECMWF model reprojected on the Sentinel-1 IW grid
wind_direction	Wind direction at 10 m height from the collocated ECMWF model reprojected on the Sentinel-1 IW grid

2.5 Product validation

We use 1-year of Doppler shift retrievals from the Sentinel-1A/B IW swaths to derive the ocean surface current RVLs along the southeastern coast of South Africa (Agulhas current) from May 2019 to April 2020. We calculated the total ocean surface RVL (i.e., combined sea state and surface current), u_{rvl}, and the ocean surface current RVL, u_{osc}, from the Doppler frequency shift and wave bias estimates provided in 898 S1-OCN-RVL products (see PUM for the processing details). The SAR-derived RVLs were systematically collocated and compared with the daily grided geostrophic velocity fields from the altimetry, satellite-derived daily Sea Surface

Temperature (SST) fields, and Lagrangian surface drifter trajectories from hourly positions (Table 4) on the case-by-case basis.

Table 4 Collocated Datasets

Sensor	Platforms	Parameters	Resolution		Provider
			Spatial	Temporal	
Synthetic Aperture Radar	Sentinel-1A/B	Doppler frequency shift	1 km	-	Copernicus, ODL, NERSC
Altimetry	S-3A, HY-2A, Saral/ AltiKa, Cryosat-2	Geostrophic velocity	0.25°	daily	CMEMS
Infrared	NOAA-18, NOAA-19, METOP-A, ENVISAT, AQUA, TRMM	SST	0.1°	daily	CMEMS
In situ drifter	SVP drifter	Drifter velocity	-	hourly	GDP

Figure 2 shows the Sentinel-1A scene acquired in the ascending pass on 7 July 2019 at 16:36:36 of the east coast of South Africa. Given that the SAR detects only the line-of-sight component of the ocean surface motion, the positive/negative RVLs in Figure 2a,b indicates the northeast/ southwestward velocity.

The gradients SAR-derived in the u_{rvl} field (Figure 2a) reveal the position of the Agulhas current propagating towards the southwest along the coast. The Agulhas current feature is also present at the same location in the geostrophic velocity field (Figure 2e) which indicates the consistence between the two independent measurements. The position of the current is also confirmed by the SST field from the same day (Figure 2f).

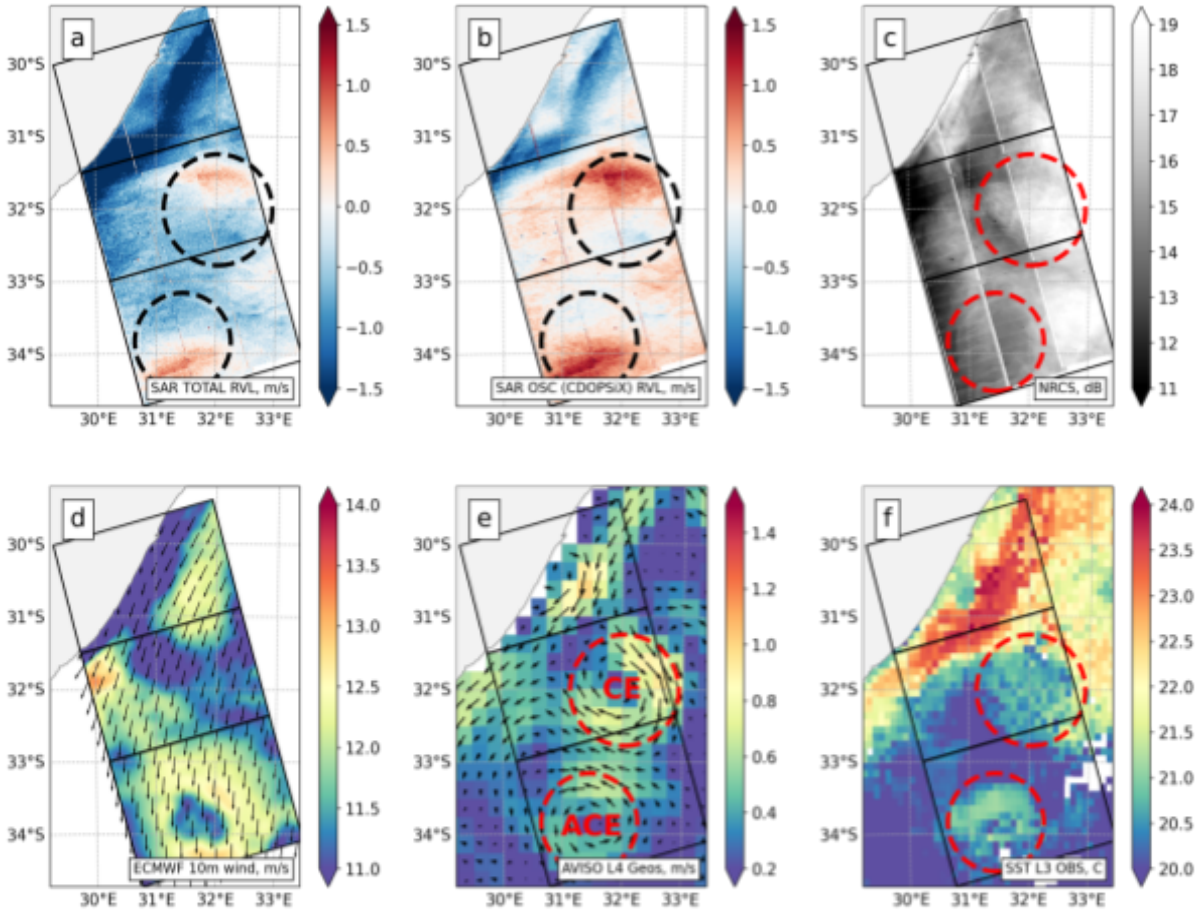

Figure 2. *The Sentinel-1A SAR scene acquired in ascending pass on 7 July 2019 at 16:36:36: (a) Total surface radial velocity (i.e., wave- and surface-current-induced signal) from the Doppler shift; (b) Ocean surface current radial velocity (i.e., after removal of the sea-state-induced signal) from the Doppler shift; (c) Normalized radar cross section. The blue/red color in a, b indicates south-westward/north-eastward velocity. The SAR scene is collocated with: (d) Wind speed (color) and direction (arrows) at 10m height from the ECMFW; (e) Geostrophic velocity from altimetry observations; (f) Satellite derived Sea Surface Temperature field. The black frames indicate footprint of the SAR acquisition frames. The dashed contours in subplots b, c, e, f represent position of the cyclonic (CE) and anticyclonic (ACE) eddies detected in the geostrophic velocity field.*

Although the surface current position can be detected in the u_{rvl} field, the signal is contaminated by the sea state bias that, in the first order, can be related to the local near-surface wind field (Figure 2d). From this imaging geometry, the wind blowing towards the south-southwest corresponds to the ocean surface motion towards the antenna yielding $u_{rvl} < 0$. Based on the estimates from the CDOPSiX the sea state bias yields RVLs from 0.4 m/s in the southern part of the scene where close to azimuth wind direction (where SAR is least sensitive to the motion) to over 1.0 m/s in the near coastal zone due to the wind of close to range direction (where SAR sensitivity is strongest). The u_{osc} field (Figure 2b) is retrieved after the removal of the sea state bias from the total signal (eq. 2). The u_{osc} field provide a clearer position of the Agulhas current compared to the the u_{rvl} field. The SAR-derived u_{osc} in the Agulhas current are up to 2 times stronger than detected in the geostrophic velocity field. First, it might be related to the fact that the SAR detects the total surface current which includes geostrophic current, wind-driven current, and wave-induced Stokes drift while altimetry derives only the geostrophic component of the surface current velocity. Second, inaccurate wave bias correction due to errors in the model wind field and CDOPSiX can yield intensification/reduction of the SAR-derived surface currents.

In addition to the main Agulhas current feature, we can also detect a mesoscale anticyclonic (ACE) and cyclonic (CE) eddy in both SAR- and altimetry-derived fields. Moreover, the expression of the ACE can be detected in the ocean surface roughness field observed by SAR (Figure 2c). Analysis of the u_{osc} field in the position of both eddies indicates that one side of the eddy (where velocities are directed towards north-east) yields a significantly stronger signal compared to the other side (where velocities are directed towards south-west). That might indicate the inaccurate removal of the wave bias. Given virtually uniform wind field over the eddy (Figure 2d) the removal of corresponding wave bias yields intensification of one part of

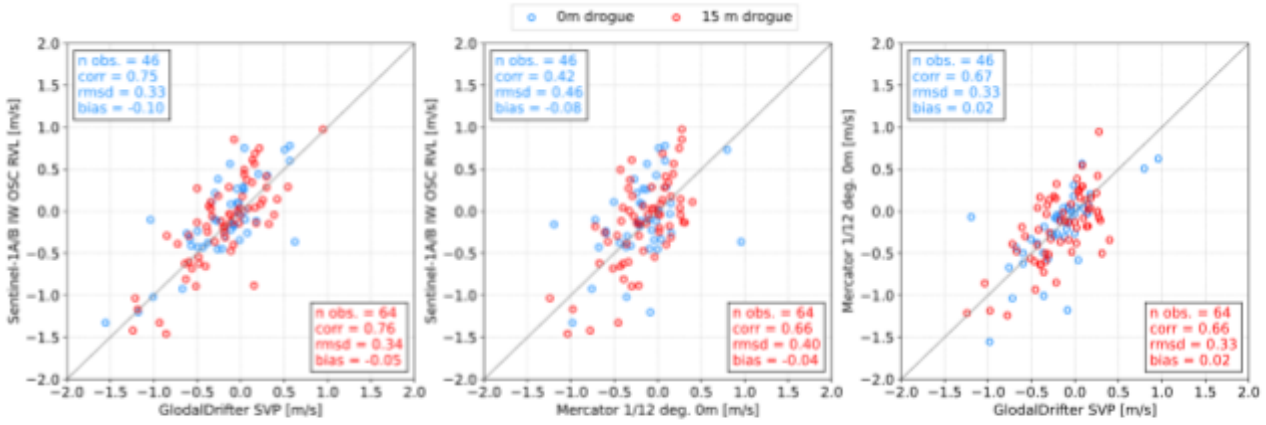

Figure 3. *Sentinel-1 A/B IW OSC RVLs in Agulhas region collocated with RVLs from 15 m drogued (red markers) and undrogued (blue markers) drifters and Mercator model: (left) SAR vs. drifters, (middle) SAR vs. Model, (right) model vs. drifters.*

the eddy and respective weakening of the other side.

The surface current features from S1-OSC-RVL products are also consistent with the in situ Lagrangian ocean surface drifter observations. We used trajectories of SVP drifters with drogue at 15 m depth and without the drogue both available trajectories from the Global Drifter

Program (GDP). As expected, drifter trajectories are consistent with ocean surface current features in SAR-derived RVL maps, especially within the Agulhas current. We also compared hourly drifter velocities [9] along the trajectory with the SAR-derived RVLs on a point-by-point basis (Figure 3). The SAR-derived RVLs are consistent with drifter-derived RVLs with the bias of 0.1 m/s and RMSD of 0.33 m/s. Notably, there is no wind slip correction applied to the drifter observations which can contribute to the disagreement. Moreover, we found that SAR, drifters, and an ocean model show similar performance in terms of the magnitude of RVL (Figure 3). All in all, based on the comparison with the independent data, S1 OSC RVL product can retrieve accurate ocean surface current radial velocity retrievals with high spatial resolution.